# Self-consistent $GW$: All-electron implementation with localized basis functions

Fabio Caruso,[1,2] Patrick Rinke,[1,2] Xinguo Ren,[1,3] Angel Rubio,[4,1,2] and Matthias Scheffler[1,2]
[1]*Fritz-Haber-Institut der Max-Planck-Gesellschaft, Faradayweg 4-6, D-14195 Berlin, Germany*
[2]*European Theoretical Spectroscopy Facility*
[3]*Key Laboratory of Quantum Information, University of Science and Technology of China, Hefei 230026, China*
[4]*Nano-Bio Spectroscopy group and ETSF Scientific Development Centre, Departamento Física de Materiales, Universidad del País Vasco, CFM CSIC-UPV/EHU-MPC and DIPC, Avenida Tolosa 72, E-20018 San Sebastián, Spain*
(Received 19 March 2013; revised manuscript received 3 May 2013; published 5 August 2013)

This paper describes an all-electron implementation of the self-consistent $GW$ (sc-$GW$) approach—i.e., based on the solution of the Dyson equation—in an all-electron numeric atom-centered orbital basis set. We cast Hedin's equations into a matrix form that is suitable for numerical calculations by means of (i) the resolution-of-identity technique to handle four-center integrals and (ii) a basis representation for the imaginary-frequency dependence of dynamical operators. In contrast to perturbative $G_0W_0$, sc-$GW$ provides a consistent framework for ground- and excited-state properties and facilitates an unbiased assessment of the $GW$ approximation. For excited states, we benchmark sc-$GW$ for five molecules relevant for organic photovoltaic applications: thiophene, benzothiazole, 1,2,5-thiadiazole, naphthalene, and tetrathiafulvalene. At self-consistency, the quasiparticle energies are found to be in good agreement with experiment and, on average, more accurate than $G_0W_0$ based on Hartree-Fock or density-functional theory with the Perdew-Burke-Ernzerhof exchange-correlation functional. Based on the Galitskii-Migdal total energy, structural properties are investigated for a set of diatomic molecules. For binding energies, bond lengths, and vibrational frequencies sc-$GW$ and $G_0W_0$ achieve a comparable performance, which is, however, not as good as that of exact-exchange plus correlation in the random-phase approximation and its advancement to renormalized second-order perturbation theory. Finally, the improved description of dipole moments for a small set of diatomic molecules demonstrates the quality of the sc-$GW$ ground-state density.

DOI: 10.1103/PhysRevB.88.075105 PACS number(s): 31.15.−p, 71.10.−w, 71.15.Qe

Many-body perturbation theory (MBPT)[1] in the $GW$ approach for the electron self-energy[2–4] provides a natural framework for an *ab initio*, parameter-free description of photo-ionization processes and charged excitations.[5] In recent years, the $GW$ approach has become a popular method for the computation of band gaps and charged excitation energies for extended[6,7] and finite systems.[8,9] In numerical implementations, following Hybertsen and Louie,[10] it is standard practice to treat the $GW$ self-energy as a single-shot perturbation ($G_0W_0$) acting on a Kohn-Sham (KS) or Hartree-Fock (HF) reference system. Thus, excitation energies are evaluated from first-order Feynman-Dyson perturbation theory as corrections to a set of single-particle eigenvalues.

The popularity of the $G_0W_0$ approximation stems from the substantial reduction in the complexity of Hedin's equations at first-order perturbation theory: The KS or HF eigenstates from a self-consistent field calculation can be used as basis functions and provide a convenient representation in which the noninteracting Green's function is diagonal. In this basis, only diagonal matrix elements of the self-energy $\Sigma$ are needed to evaluate quasiparticle corrections at first order. Thus, $G_0W_0$ grants a considerable simplification of the linear algebra operations which is decisive for applying the theory to large molecules and solids.

Although numerically more efficient than a nonperturbative approach, $G_0W_0$ suffers from several undesirable shortcomings such as the dependence on the starting point;[7,11–13] the violation of conservation laws for momentum, total energy, and particle number;[14–16] and—most importantly—the limited access to ground-state properties, which are kept unchanged from the preliminary density functional theory (DFT) or HF calculations.

It is known that the self-consistent $GW$ approach (sc-$GW$)—in which both the Green's function $G$ and the screened Coulomb interaction $W$ are iterated to self-consistency—ameliorates most of the pathologies of perturbative $G_0W_0$.[17] A particularly appealing feature of the sc-$GW$ method is the possibility of treating ground and excited states *at the same level of theory*. This property arises by virtue of the nonperturbative nature of the sc-$GW$ approach, whereby the Green's function is updated and encompasses many-body effects introduced by the self-energy. In contrast, in perturbative theories (which generally do not introduce updates in the Green's function) the electronic structure coincides with that of the corresponding starting point. Therefore, density and total energy—and derived quantities such as dipole moments, bond lengths, and binding energies—become accessible at self-consistency and reveal the quality of the $GW$ ground state. Finally, at self-consistency excited- and ground-state properties are independent of the starting point, at least for closed-shell systems,[17] and provide an *unbiased* assessment of the $GW$ approach.

A previous study on the homogeneous electron gas (HEG) reported a deterioration of the sc-$GW$ spectral properties, as compared to $G_0W_0$.[18] This has been attributed to a poor description of the satellite peaks at self-consistency.[18] For extended systems, the performance of sc-$GW$ remains controversial due to the scarce number of calculations for real solids.[19–22] Part of this controversy can be traced back to basis set problems in early all-electron calculations[23] and to the

 

large influence that pseudopotentials may have on $GW$ band gaps.[24] More recently, sc-$GW$ calculations for atoms[25] and molecules[9,17] have shown improvements in the description of the first ionization energies and for transport properties[26] of finite systems.

The price to pay in sc-$GW$ is the demanding iterative procedure. The higher complexity of sc-$GW$ arises for the following reasons. (i) The Green's function obtained from the solution of the Dyson equation is, in general, nondiagonal. This considerably increases the computational cost of the evaluation of the dielectric matrix. (ii) The nondiagonal matrix elements of $\Sigma$ are needed to solve the Dyson equation. (iii) Dynamical quantities require Fourier transforms, that introduce their own computational difficulties.

In the first part of this paper, we present an all-electron implementation of the sc-$GW$ method in the localized basis-set code FHI-AIMS[27] and propose a recipe to efficiently address points (i)–(iii). An optimized set of localized basis functions was used to represent the Green's function and the self-energy operator. Nonlocal two-particle operators, such as the screened Coulomb interaction, were computed by means of the resolution of the identity technique[28–30] (also known as the density fitting method) in a general framework previously introduced by some of us.[31] Finally, an auxiliary basis of Lorentzian functions was introduced for an efficient analytical evaluation of Fourier transforms between imaginary time and frequency.

The second part of the paper focuses on the assessment of ground- and excited-state properties as obtained from sc-$GW$ for molecules. The quality of the sc-$GW$ ground state was investigated by computing binding energies, bond lengths, vibrational frequencies, densities, and dipole moments for a small set of hetero- and homoatomic dimers. The full valence excitation spectra were evaluated for a set of molecules relevant for organic photovoltaic applications (thiophene, benzoithiazole, 1,2,5-thiadiazole, naphthalene, and tetrathiafulvalene). From this study we conclude that sc-$GW$ systematically improves the spectral properties of finite systems over the entire excitation spectrum (that is, not only for the first ionization energy) as compared to standard perturbative $G_0W_0$ calculations based on semilocal DFT and HF. Nonetheless, for certain starting points—exemplified by the PBE0 hybrid functional—$G_0W_0$ slightly outperforms sc-$GW$, providing ionization energies in better agreement with experimental reference data, as also previously demonstrated for benzene and the azabenzenes in Ref. 12. For structural properties the sc-$GW$ method yields a less satisfactory agreement with experiment. For dimers, bond lengths and binding energies are slightly underestimated, and in this case there is no substantial improvement over perturbative approaches such as $G_0W_0$ or the random-phase approximation (RPA). Finally, self-consistency gives an accurate description of the electron density as manifested by the accurate dipole moments of diatomic molecules. These results suggest that sc-$GW$ is a promising method for charge transfer compounds and interfaces. However, our study also indicates the importance of including higher order exchange and correlation diagrams beyond $GW$ to accurately describe the structural properties of molecules.

The paper is organized as follows. Section I gives a brief introduction to the $GW$ approximation, recalling the basic equations needed for the computation of the Green's function $G$ and the self-energy $\Sigma$. An optimal representation of Hedin's equations in terms of localized basis functions and of the resolution of the identity is presented in Sec. II. In Sec. III we present the scheme employed in the computation of the Fourier integrals of the Green's function and other dynamical quantities. We report in Sec. IV an assessment of sc-$GW$ for the excitation spectra of molecules and, in Sec. V, for the ground-state properties of diatomic molecules. Our conclusions and final remarks are reported in Sec. VI.

## I. THEORETICAL FRAMEWORK

In MBPT the complexity of the many-body problem is recast into the calculation of the single-particle Green's function. Knowledge of the Green's function grants immediate access to the (charged) single-particle excitation energies of the system, to the total energy, and, more generally, to expectation values of any single-particle operator. Green's function theory is well documented in the literature[1] and we recall here only the basic equations relevant for the $GW$ approach, adhering to Hartree atomic units $\hbar = m_e = e^2 = 1$.

For a system of noninteracting electrons described through a time-independent Hamiltonian, the Green's function can be written explicitly in terms of the single-particle eigenstates $\psi_n^\sigma(\mathbf{r})$ and eigenvalues $\epsilon_n^\sigma$,

$$G_0^\sigma(\mathbf{r},\mathbf{r}',\omega) = \sum_n \frac{\psi_n^\sigma(\mathbf{r})\psi_n^{\sigma*}(\mathbf{r}')}{\omega - \left(\epsilon_n^\sigma - \mu\right) - i\eta\,\mathrm{sgn}\left(\mu - \epsilon_n^\sigma\right)}, \qquad (1)$$

where $n$ and $\sigma$ refer to orbital and spin quantum numbers, respectively. $\mu$ is the electron chemical potential, and $\eta$ a positive infinitesimal. In practice, $\psi_n^\sigma(\mathbf{r})$ and $\epsilon_n^\sigma$ are generally obtained from the self-consistent solution of the HF or (generalized) KS equations.

For interacting electrons, the Green's function has to be evaluated by solving the Dyson equation:

$$\begin{aligned} G^\sigma(\mathbf{r},\mathbf{r}',\omega) = G_0^\sigma(\mathbf{r},\mathbf{r}',\omega) + \int d\mathbf{r}_1 d\mathbf{r}_2 G_0^\sigma(\mathbf{r},\mathbf{r}_1,\omega) \\ \times \left[\Sigma^\sigma(\mathbf{r}_1,\mathbf{r}_2,\omega) + \Delta v_{\mathrm{H}}^\sigma(\mathbf{r}_1)\delta(\mathbf{r}_1-\mathbf{r}_2) \right. \\ \left. - v_{\mathrm{xc}}^\sigma(\mathbf{r}_1,\mathbf{r}_2)\right] G^\sigma(\mathbf{r}_2,\mathbf{r}',\omega). \end{aligned} \qquad (2)$$

Here $\Delta v_{\mathrm{H}}^\sigma$ is the change in the Hartree potential accounting for density differences between $G_0^\sigma$ and $G^\sigma$ and $v_{\mathrm{xc}}^\sigma$ is the exchange-correlation part of the single-particle Hamiltonian corresponding to the noninteracting Green's function $G_0$. For example, if $G_0$ is the HF Green's function, then $v_{\mathrm{xc}}^\sigma$ corresponds to the nonlocal exchange operator $\Sigma_{\mathrm{x}}$. Alternatively, for a KS Green's function, $v_{\mathrm{xc}}^\sigma$ is the local exchange-correlation potential. The electron self-energy $\Sigma^\sigma$ encompasses all many-body exchange-correlation effects and therefore its practical evaluation requires approximations. Following Hedin,[2,5] the self-energy can be expanded in a perturbative series of the *screened* Coulomb interaction $W$, with the first-order term given by the $GW$ approximation:

$$\Sigma^\sigma(\mathbf{r},\mathbf{r}',\tau) = iG^\sigma(\mathbf{r},\mathbf{r}',\tau)W(\mathbf{r},\mathbf{r}',\tau). \qquad (3)$$

By virtue of the time translation invariance it suffices to express $\Sigma$ in terms of time differences ($\tau = t - t'$). The screened interaction $W(\mathbf{r},\mathbf{r}',\omega)$ is, in turn, defined through another

Dyson equation:

$$W(\mathbf{r},\mathbf{r}',\omega) = v(\mathbf{r},\mathbf{r}') + \int d\mathbf{r}_1 d\mathbf{r}_2 v(\mathbf{r},\mathbf{r}_1)\chi(\mathbf{r}_1,\mathbf{r}_2,\omega) \times W(\mathbf{r}_2,\mathbf{r}',\omega). \quad (4)$$

Here, $v$ is the bare Coulomb interaction $1/|\mathbf{r}-\mathbf{r}'|$ and $\chi$ the irreducible polarizability, which in $GW$ is approximated by the product of two Green's functions:

$$\chi(\mathbf{r},\mathbf{r}',\tau) = -i\sum_\sigma G^\sigma(\mathbf{r},\mathbf{r}',\tau)G^\sigma(\mathbf{r}',\mathbf{r},-\tau). \quad (5)$$

The self-consistent nature of Eqs. (2)–(5) arises from the interdependence of the self-energy and the Green's function. In the $G_0W_0$ approach, the self-energy is evaluated non-self-consistently, and the Dyson equation is solved approximately in a perturbative fashion. The quasiparticle excitation energies are then obtained from the quasiparticle equation:

$$\epsilon^{\mathrm{QP}}_{n,\sigma} = \epsilon^\sigma_n + \mathrm{Re}\langle\psi^\sigma_n|\Sigma^\sigma\left(\epsilon^{\mathrm{QP}}_{n,\sigma}\right) - v^\sigma_{\mathrm{xc}}|\psi^\sigma_n\rangle. \quad (6)$$

In this work, Eqs. (2)–(5) are solved fully self-consistently. In practice, an iterative procedure requires the following steps:

(1) construction of an initial noninteracting Green's function $G_0$ from a preliminary SCF calculation through Eq. (1);

(2) evaluation of the polarizability $\chi$ from Eq. (5) and Fourier transformation of $\chi$ to the frequency domain;

(3) calculation of the screened Coulomb interaction $W$ from Eq. (4) and Fourier transformation of $W$ to the time domain;

(4) evaluation of the self-energy $\Sigma$ from the Eq. (3) and Fourier transformation of $\Sigma$ to the frequency domain;

(5) update of the Green's function from the Dyson equation [Eq. (2)] and Fourier transformation of $G$ to the time domain;

(6) mixing of the Green's function to accelerate the convergence of the self-consistent loop;

(7) iteration of steps (2)–(6) until a convergence criterion is satisfied.

In a numerical implementation, a choice for the basis set expansion of the quantities in Eqs. (2)–(5) has to be made. Our choice is discussed in the next section.

## II. SELF-CONSISTENT *GW* WITHIN A LOCALIZED BASIS

Previous implementations of sc-$GW$ were based on Gaussians or Slater orbitals,[18,25] full potential linear augmented plane waves,[20,21] real-space grids,[32] and numeric atom-centered orbitals (NAOs).[9] In the present work, the Green's function $G$, the self-energy $\Sigma$, and all single-particle operators, are expanded in a NAO basis $\{\varphi_i(\mathbf{r})\}$, with basis functions of the form

$$\varphi_i(\mathbf{r}) = \frac{u_i(r)}{r}Y_{lm}(\Omega), \quad (7)$$

where $u_i(r)$ are numerically tabulated radial functions and $Y_{lm}(\Omega)$ spherical harmonics. For numerical convenience, we work with real-valued basis functions by requiring—without loss of generality—that $Y_{lm}(\Omega)$ denotes the real part (for $m = 0,\ldots,l$) and the imaginary part (for $m = -l,\ldots,-1$) of complex spherical harmonics. In FHI-AIMS the choice of the radial functions $u_i(r)$ is not limited. In this work we show results for numerically tabulated Gaussian orbital basis sets and the *Tier* hierarchy of FHI-AIMS for NAOs.[27] We refer to Ref. 27 for details on the construction and optimization as well as the properties of the NAO basis sets in FHI-AIMS.

In terms of the $\varphi_i$ basis functions, the Green's function can be expanded as

$$G^\sigma(\mathbf{r},\mathbf{r}',i\omega) = \sum_{ijlm}^{N_{\mathrm{basis}}}\varphi_i(\mathbf{r})s^{-1}_{ij}G^\sigma_{jl}(i\omega)s^{-1}_{lm}\varphi_m(\mathbf{r}'), \quad (8)$$

where $s_{ij} = \int d\mathbf{r}\varphi_i(\mathbf{r})\varphi_j(\mathbf{r})$ is the overlap matrix taking into account the nonorthonormality of the basis set and $N_{\mathrm{basis}}$ is the total number of basis functions. In the following, sums over Latin indices $i,j,l,m$ are implicitly assumed to run from 1 to $N_{\mathrm{basis}}$, whereas sums over $n$ run over the total number of states. The coefficients $G^\sigma_{ij}(i\omega)$ of the expansion are given by

$$G^\sigma_{ij}(i\omega) = \int d\mathbf{r}d\mathbf{r}'\varphi_i(\mathbf{r})G^\sigma(\mathbf{r},\mathbf{r}',i\omega)\varphi_j(\mathbf{r}'). \quad (9)$$

The representation in Eq. (9) can be easily applied to the noninteracting Green's function in Eq. (1), yielding

$$G^\sigma_{0,ij}(i\omega) = \sum_n\sum_{lm}\frac{s_{il}c^\sigma_{ln}c^\sigma_{mn}s_{mj}}{i\omega-\left(\epsilon^\sigma_n-\mu\right)}, \quad (10)$$

where we introduced the expansion of the HF/KS orbitals in the NAO basis $\psi^\sigma_n(\mathbf{r}) = \sum_l c^\sigma_{ln}\varphi_l(\mathbf{r})$ and the Green's function was continued to the imaginary frequency axis. The matrix representation in Eq. (9) is also adopted for the Hartree potential $v^\sigma_{\mathrm{H}}$, the self-energy $\Sigma^\sigma$, and the exchange-correlation potential $v^\sigma_{\mathrm{xc}}$. We emphasize that in our implementation the summation over empty states—which is at the origin of the basis-set convergence problem of $GW$ calculations[33–36]—enters only through Eq. (10). The self-energy and the polarizability are evaluated as functionals of the Green's function, and therefore do not involve any explicit empty-state summation.

To rewrite Hedin's equations in a matrix form suitable for a numerical implementation, we need to introduce a matrix representation for two-particle operators. The expansion of two-particle operators in a numerical basis cannot be handled efficiently through Eq. (9) due to the appearance of the four-orbital two-electron Coulomb integrals of the form

$$(ij|kl) = \int\frac{\varphi_i(\mathbf{r})\varphi_j(\mathbf{r})\varphi_k(\mathbf{r}')\varphi_l(\mathbf{r}')}{|\mathbf{r}-\mathbf{r}'|}d\mathbf{r}d\mathbf{r}'. \quad (11)$$

The computation of the Coulomb repulsion integrals in Eq. (11) is a problem extensively discussed in the literature[33,37–44] and efficient techniques have been developed over the years to make this calculation affordable. Numerically, the difficulty arises from the large number of NAO pairs and from the memory requirements of storing the four-index matrix $(ij|kl)$. In the NAO framework, the integrals in Eq. (11) are often evaluated by introducing an auxiliary basis set $\{P_\mu(\mathbf{r})\}$, with basis functions $P_\mu(\mathbf{r})$ defined to span the Hilbert space of NAO pairs,

$$\varphi_i(\mathbf{r})\varphi_j(\mathbf{r}) \simeq \sum_{\mu=1}C^\mu_{ij}P_\mu(\mathbf{r}), \quad (12)$$

where $C^\mu_{ij}$ are the coefficients of the expansion. Due to the high linear dependence of the NAO products, the number of product basis functions $N_{\mathrm{aux}}$ is much smaller than the number of NAO pairs $O(N^2_{\mathrm{basis}})$, making the numerical evaluation of

Eq. (11) affordable. This technique, known as the *resolution of the identity* (RI)—or also density-fitting technique—was implemented in the FHI-AIMS code and we refer to Ref. 31 for a detailed account of the variational approach employed in the determination of the RI coefficients $C_{ij}^{\mu}$ and for a review of the overall accuracy of the RI approach for correlated calculations.

In short, we used the "RI-V" variant of the RI scheme, in which the expansion coefficients are given by

$$C_{ij}^{\mu} = \sum_{\nu} (ij|\nu) V_{\nu\mu}^{-1}, \tag{13}$$

where $(ij|\nu) \equiv \int d\mathbf{r} \varphi_i(\mathbf{r}) \varphi_j(\mathbf{r}) P_{\mu}(\mathbf{r}')/|\mathbf{r}-\mathbf{r}'|$ and $V_{\nu\mu}$ denotes matrix elements of the Coulomb matrix in the auxiliary basis, i.e., $V_{\mu\nu} = \int d\mathbf{r} d\mathbf{r}' P_{\mu}(\mathbf{r}) P_{\nu}(\mathbf{r}')/|\mathbf{r}-\mathbf{r}'|$. For numerical efficiency, it is convenient to work with the generalized coefficients:

$$M_{ij}^{\mu} = \sum_{\nu} C_{ij}^{\nu} V_{\nu\mu}^{1/2}. \tag{14}$$

Following Ref. 31, one can write the RI version of the Dyson equation for the screened Coulomb interaction [Eq. (4)] as

$$\overline{W}_{\mu\nu}(i\omega) \equiv [v^{-1} W(i\omega)]_{\mu\nu} = [1 - \Pi(i\omega)]_{\mu\nu}^{-1}, \tag{15}$$

where we defined $[\Pi(i\omega)]_{\mu\nu} \equiv [\chi(i\omega) v]_{\mu\nu}$. In contrast to the RI-based implementation of the $G_0W_0$ method,[31] the operator $\Pi$ has to be expressed as an explicit functional of $G$. Moreover, all nondiagonal matrix elements in the Green's function have to be included. These two criteria are satisfied by evaluating $\Pi$ in terms of the $M_{ij}^{\mu}$ coefficients as

$$[\Pi(i\tau)]_{\mu\nu} = -i \sum_{\sigma} \sum_{ijlm} M_{il}^{\mu} M_{jm}^{\nu} \overline{G}_{ij}^{\sigma}(i\tau) \overline{G}_{lm}^{\sigma}(-i\tau). \tag{16}$$

Here we defined

$$\overline{G}_{ij}(i\tau) \equiv \sum_{lm} s_{il}^{-1} G_{lm}(i\tau) s_{mj}^{-1}. \tag{17}$$

The quadruple sum in Eq. (16) may be reduced to double sums—with a considerable reduction of computational cost—by introducing the intermediate quantity $A_{lj,\sigma}^{\mu}(i\tau) \equiv \sum_i M_{il}^{\mu} \overline{G}_{ij}^{\sigma}(i\tau)$. In terms of these coefficients, Eq. (16) becomes

$$[\Pi(i\tau)]_{\mu\nu} = -i \sum_{\sigma} \sum_{lj} A_{lj,\sigma}^{\mu}(i\tau) A_{jl,\sigma}^{\nu}(-i\tau). \tag{18}$$

The self-energy can be evaluated in terms of Eq. (15) providing the following matrix representation of Eq. (3):

$$\Sigma_{ij}^{\sigma}(i\tau) = \frac{i}{2\pi} \sum_{lm} \sum_{\mu\nu} M_{il}^{\mu} M_{jm}^{\nu} \overline{G}_{lm}^{\sigma}(i\tau) \overline{W}_{\mu\nu}(i\tau). \tag{19}$$

By introducing the auxiliary quantity $B_{jm}^{\mu}(i\tau) = \sum_{\nu} M_{jm}^{\nu} \overline{W}_{\mu\nu}(i\tau)$, the self-energy can again be cast into a double-sum form:

$$\Sigma_{ij}^{\sigma}(i\tau) = \frac{i}{2\pi} \sum_{m} \sum_{\mu} A_{im,\sigma}^{\mu}(i\tau) B_{jm}^{\mu}(i\tau). \tag{20}$$

The correlation (exchange) contribution to the self-energy can be derived straightforwardly from Eq. (19) by substituting $\overline{W}$ with $\overline{W}_{\mu\nu}^{c} \equiv \overline{W}_{\mu\nu} - \delta_{\mu\nu}$ ($\overline{W}_{\mu\nu}^{x} \equiv \delta_{\mu\nu}$). The Hartree potential $v_{H}^{\sigma}$ is also evaluated as an explicit functional of $G$ as

$$v_{H,ij}^{\sigma} = \sum_{lm} \sum_{\mu} M_{ij}^{\mu} M_{lm}^{\mu} \overline{G}_{lm}^{\sigma}(i\tau = 0^{-}). \tag{21}$$

Finally, the matrix representation of the Dyson equation for the Green's function completes the set of Hedin's equations:

$$\overline{G}_{ij}^{\sigma}(i\omega) = \left[\overline{G}_{0}^{\sigma}(i\omega)^{-1} - \Sigma^{\sigma}(i\omega) + v_{xc}^{\sigma} - \Delta v_{H}^{\sigma}\right]_{ij}^{-1}. \tag{22}$$

Here $\Delta v_{H}^{\sigma}$ is the difference between the Hartree potential of the interacting and the noninteracting Green's function.

To facilitate the convergence of the sc-$GW$ loop, the input Green's function $\overline{G}^{\text{input}}$ of the $(N+1)$th iteration is obtained from a linear mixing scheme,

$$\overline{G}_{ij}^{\text{input}}(i\tau) = \alpha \overline{G}_{ij}^{N}(i\tau) + (1-\alpha) \overline{G}_{ij}^{N-1}(i\tau), \tag{23}$$

where $\overline{G}^{N}$ denotes the Green's function obtained from the $N$th solution of the Dyson equation, and $\alpha$ is the mixing parameter. As illustrated in panel (b) of Fig. 1, we find that $\alpha = 0.2$ is typically a good choice. The convergence of the self-consistent loop is monitored looking at the average deviation of the Green's function at each iteration $\Delta$, defined as

$$\Delta = \frac{1}{N_{\text{basis}}^2} \sum_{i,j} \left| \overline{G}_{ij}^{N}(i\tau = 0^{-}) - \overline{G}_{ij}^{N-1}(i\tau = 0^{-}) \right|. \tag{24}$$

The sc-$GW$ loop is considered converged when $\Delta$ drops below a chosen threshold $\Delta_{\text{th}}$. Default settings used in most calculations are $\Delta_{\text{th}} = 10^{-5}$, which suffices to converge both total and quasiparticle energies. The convergence of sc-$GW$ is illustrated in the left panel of Fig. 1, where $\Delta$ is reported as a function of the number of iterations for $H_2$, $H_2O$, and $C_6H_6$.

Equations (15)–(22) constitute a matrix representation of Hedin's equations in the $GW$ approach [Eqs. (2)–(5)]. We emphasize again that in Eqs. (15)–(22) (i) all electrons are treated on the same quantum mechanical level, i.e., fully self-consistently; (ii) no model screening was used in the calculation of $W$; (iii) all nondiagonal matrix elements of $G$ and $\Sigma$ are correctly accounted for.

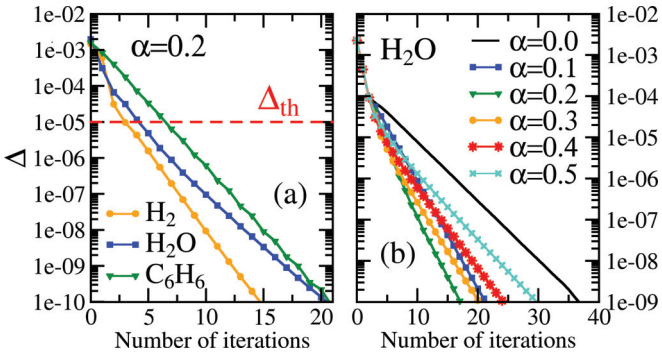


FIG. 1. (Color online) (a) Values of $\Delta$—defined in Eq. (24)—as a function of the number of iterations of the sc-$GW$ loop for $H_2$, $H_2O$, and $C_6H_6$ in their equilibrium geometry in a Tier 2 basis set. A linear mixing parameter $\alpha = 0.2$ was used for all molecules. $\Delta_{\text{th}}$ indicates the default value of the convergence threshold. (b) Values of $\Delta$ for $H_2O$ as a function of the number of iterations for different values of $\alpha$.

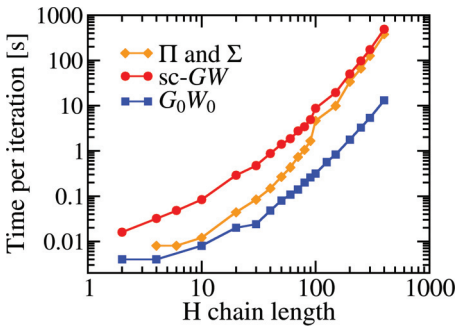


FIG. 2. (Color online) Total time (in seconds, on a single CPU) per iteration of the sc-$GW$ loop for linear hydrogen chains of different lengths. The total time required for the evaluation of the self-energy in $G_0W_0$ is included for comparison.

The evaluation of Eqs. (16) and (19) is the most computationally demanding operation of our implementation. The scaling of the computational time as a function of the basis set size equals that of $G_0W_0$ calculations but with a larger prefactor. To illustrate this aspect, we report in Fig. 2 the total computational time spent for a single iteration of Eqs. (15)–(22) as function of the length of a linear hydrogen chain in a minimal basis set (i.e., with one NAO per atom). As compared to conventional $G_0W_0$ implementations, the additional computational cost arises from the necessity of accounting for nondiagonal matrix elements in the calculation of $G$ and $\Sigma$.

The only approximation introduced up to this point is the RI for the expansion of the product of NAO pairs [Eq. (12)]. As discussed in Ref. 31, the accuracy of the RI can be monitored systematically by means of two control parameters: $\varepsilon_{\text{orth}}$ and $\varepsilon_{\text{SVD}}$. $\varepsilon_{\text{orth}}$ sets the accuracy threshold for the Gram-Schmidt orthonormalization employed for the reduction of the linear dependence of on-site (i.e., on the same atom) product basis functions $P_\mu$. In practice, by choosing smaller values of $\varepsilon_{\text{orth}}$ one may increase the number of product basis functions used in the expansion in Eq. (12). Similarly, the parameter $\varepsilon_{\text{SVD}}$ controls the singular value decomposition (SVD) for the orthonormalization of product basis functions on different atoms. A more detailed description of the effects of these parameters can be found in Ref. 31. To show the effect of the RI scheme on the self-consistent Green's function, we report in Fig. 3 the sc-$GW$ total energy—evaluated from Eq. (31), introduced in Sec. V—of the water molecule as a function of

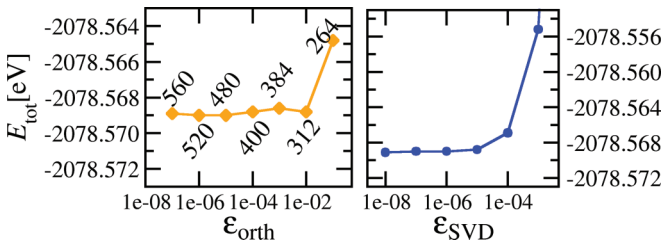


FIG. 3. (Color online) sc-$GW$ total energy of $H_2O$ as a function of the convergence parameters $\varepsilon_{\text{orth}}$ (left) and $\varepsilon_{\text{SVD}}$ (right), evaluated with a Tier 2 basis set. The number of product basis functions corresponding to each value of $\varepsilon_{\text{orth}}$ is also reported.

$\varepsilon_{\text{orth}}$ (left panel) and $\varepsilon_{\text{SVD}}$ (right panel). For a wide range of values of the control parameters $\varepsilon_{\text{orth}}$ and $\varepsilon_{\text{SVD}}$, the changes of the total energy are of the order of $10^{-4}$ eV or less. In all following calculations we therefore used $\varepsilon_{\text{orth}} = 10^{-5}$ and $\varepsilon_{\text{SVD}} = 10^{-5}$.

## III. DISCRETIZATION OF THE FOURIER INTEGRALS

In this implementation, we solve Eqs. (15)–(22) in imaginary time and frequency, taking advantage of the reduced number of frequency points required to describe $G^\sigma(i\omega)$ and other dynamical quantities, as compared to real-frequency implementations. In a mixed time-frequency formalism convolutions on the frequency axis can be expressed, by virtue of the convolution theorem, as products on the time axis after a Fourier transform. Due to the slow decay of $G^\sigma(i\omega)$ at large frequencies, the computation of Fourier transforms may require extended and dense frequency grids. We obviate this problem by introducing a basis for the frequency/time dependence of all dynamical quantities. This permits an analytic evaluation of the Fourier integrals—as one can choose basis functions with a Fourier transform known analytically—and substantially reduces the number of frequency points needed to converge the calculation.

Following the approach introduced in Ref. 45, we expand the Green's function in a set of Lorentzian functions of the form $f_n(i\omega) = 1/(b_n + i\omega)$, with Fourier transform $f(i\tau) = 1/(2\pi)e^{-b_n\tau}$. The parameters $b_n$ are fixed at the beginning of the calculation and are distributed logarithmically in the energy range covered by the KS or HF eigenvalues $\epsilon_n^\sigma$. Although, in principle, other functions could be used, the functions $f_n(i\omega)$ constitute a natural choice for the expansion of the Green's function, as the frequency dependence of $f_n(i\omega)$ closely resembles the analytic structure of $G$ and captures the $1/i\omega$ behavior at large frequency. This is illustrated in Fig. 4, where the real and imaginary parts of $f_n(i\omega)$—with different values of $b_n$—are compared to a Green's function matrix element for the Ne atom. The Green's function can be

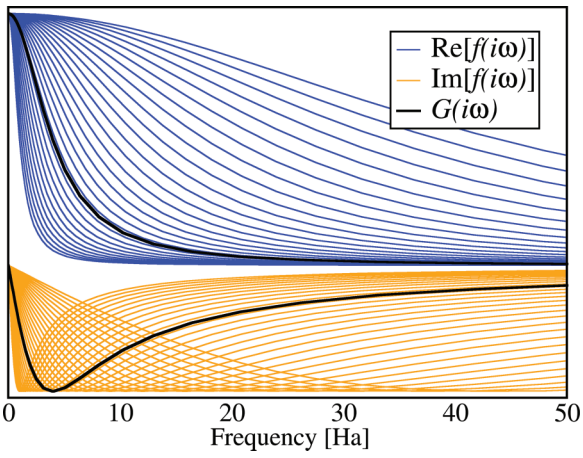


FIG. 4. (Color online) Comparison of the analytic structure of the real (in blue, top) and imaginary parts (in orange, bottom) of $f_n(i\omega)$ for different values of $b_n$ and a matrix element of the Green's function (black).

expanded in the basis of Lorentzian functions as

$$G_{ij}^{\sigma}(i\omega) = \sum_{n=1}^{N_{\text{poles}}} \left[\alpha_{ij}^{n} f_n^{\text{Re}}(i\omega) + \beta_{ij}^{n} f_n^{\text{Im}}(i\omega)\right], \qquad (25)$$

where $N_{\text{poles}}$ denotes the number of functions $f_n$ and $f_n^{\text{Re (Im)}}(i\omega)$ denotes the real (imaginary) part of $f_n(i\omega)$. The real and imaginary part of the Green's function have been treated separately to maintain a real-valued linear least-square problem, leading in turn to real-valued coefficients $\alpha_n$ and $\beta_n$. Since the Fourier transform of the $f_n(i\omega)$ is known, the coefficients $\alpha_n$ and $\beta_n$ also determine the expansion of the Green's function in imaginary time. Expansions similar to Eq. (25) were employed also for the Fourier transform of $\chi$, $W$, and $\Sigma$.

The imaginary time and frequency axes are then discretized on exponentially spaced grids composed of $N_\omega$ points in the range $\{0,\omega_{\text{max}}\}$ and by $2N_\tau + 1$ points in the range $\{-\tau_{\text{max}},\tau_{\text{max}}\}$. The grid points $\omega_n$ and integration weights $w(\omega_n)$ are defined as

$$\omega_k = \omega_0[e^{(k-1)h} - 1], \quad w(\omega_k) = h\omega_0 e^{(k-1)h}, \qquad (26)$$

and similarly for $\tau_k$ and $w(\tau_k)$. The constant $h$ is obtained by imposing the maximum frequency $\omega_{\text{max}}$ from the constraint $\omega_{\text{max}} = \omega_0[e^{N_\omega h} - 1]$ and the parameter $\omega_0$ sets the initial spacing of the grid. Typical values adopted in our calculations are $\omega_{\text{max}} = 5000$ Ha, $\tau_{\text{max}} = 1000$ Ha$^{-1}$, and $\omega_0 = \tau_0 = 0.001$.

The error introduced by the Fourier transform can be quantified for functions known analytically on both the (imaginary) frequency and time axes such as, for instance, the noninteracting Green's function given in Eq. (1). In Fig. 5, we report the mean absolute error (MAE) in the Fourier transform of the noninteracting Green's function $G_0^{\sigma}(i\omega)$ of the nitrogen dimer $N_2$, averaged over all matrix elements. The MAE drops exponentially when increasing the number of functions $f_n$, and few tens of frequency points suffice to converge the Fourier integrals with an accuracy of the order of $10^{-8}$. In our calculations we used $N_\omega = N_\tau = 60$ as default parameters.

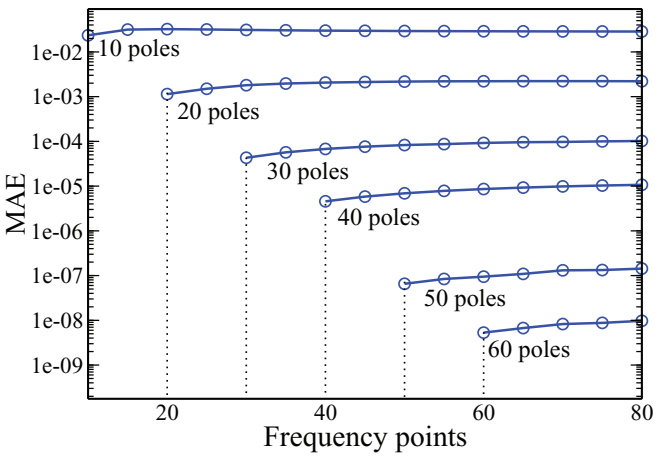


FIG. 5. (Color online) Mean absolute error (MAE) introduced by Fourier transforming the Green's function of $N_2$ for different numbers of poles and frequency points.

## IV. SPECTRAL PROPERTIES OF MOLECULES

We turn now to the spectral properties in sc-$GW$. At self-consistency, the excitation spectrum is given by the spectral function

$$\begin{aligned} A(\omega) &= -1/\pi \int d\mathbf{r} \lim_{\mathbf{r}'\to\mathbf{r}} \text{Im } G(\mathbf{r},\mathbf{r}',\omega) \\ &= -1/\pi \text{ Tr}[\text{Im } G(\omega)], \end{aligned} \qquad (27)$$

where the Green's function has to be evaluated on the real-frequency axis. To evaluate Eq. (27), we first obtain the real-frequency self-energy by means of the analytic continuation based on a two-pole fitting scheme.[46] In this approach, the matrix elements of the self-energy in the imaginary frequency domain [i.e., the Fourier transform of Eq. (20)] are fit by polynomials of the form

$$\Sigma(i\omega) \simeq \sum_{n=1}^{2} \frac{a_n}{i\omega + b_n}. \qquad (28)$$

Here the matrix element indices were suppressed for notational simplicity and the coefficients $a_n$ and $b_n$ are determined by means of a nonlinear least-square fit, solved with a Levenberg-Marquardt algorithm. By replacing $i\omega$ with $\omega$ in Eq. (28) the self-energy can then be evaluated on the real-frequency axis. Once the real-frequency self-energy is obtained, the Dyson equation is solved directly in real frequency on a fine, equally spaced grid. The resulting Green's function is used to determine the sc-$GW$ spectral function $A(\omega)$.

Previous works[46] have indicated that the two-pole model presented in Eq. (28) reliably reproduce quasiparticle energies with an average relative error of the 0.2% for solids. The parameter $\eta$ in the denominator of Eq. (1), necessary to avoid the numerical divergence of $G_0$ is set to $\eta = 10^{-4}$. This parameter contributes negligibly to the broadening of the spectral function and has no effect on the position of the quasiparticle peaks.

As an example, we report the sc-$GW$ spectral functions of $H_2O$, $NH_3$, and $N_2$ in Fig. 6 calculated using basis sets of increasing size. The sc-$GW$ spectral function shows sharp $\delta$-function-like peaks at the quasiparticle energies. The absence of broadening in the quasiparticle peaks in Fig. 6 may be associated with an infinite lifetime of the corresponding quasiparticle states, as expected for states close to the Fermi energy. As discussed in Sec. IV A, higher energy excitations may decay through the formation of electron-hole pairs, leading to a finite lifetime and thus to a more pronounced broadening of the quasiparticle peaks. In panels (a), (b), and (c) in Fig. 6 we report the spectral function corresponding to the highest occupied quasiparticle states evaluated with a Tier 1, Tier 2, and Tier 3 basis; panels (d), (e), and (f) show the peaks corresponding to the lowest unoccupied quasiparticle states. The $G_0W_0$@HF and sc-$GW$ ionization energies are reported in panels (g), (h), and (i) of Fig. 6 as a function of the basis set size. The $G_0W_0$ ionization energy is calculated from the linearized quasiparticle equation [Eq. (6)], whereas in sc-$GW$ it is extracted from the highest (valence) peak of the spectra shown in panels (a), (b), and (c).

For the quasiparticle energies corresponding to occupied states, the largest change is observed going from Tier 1

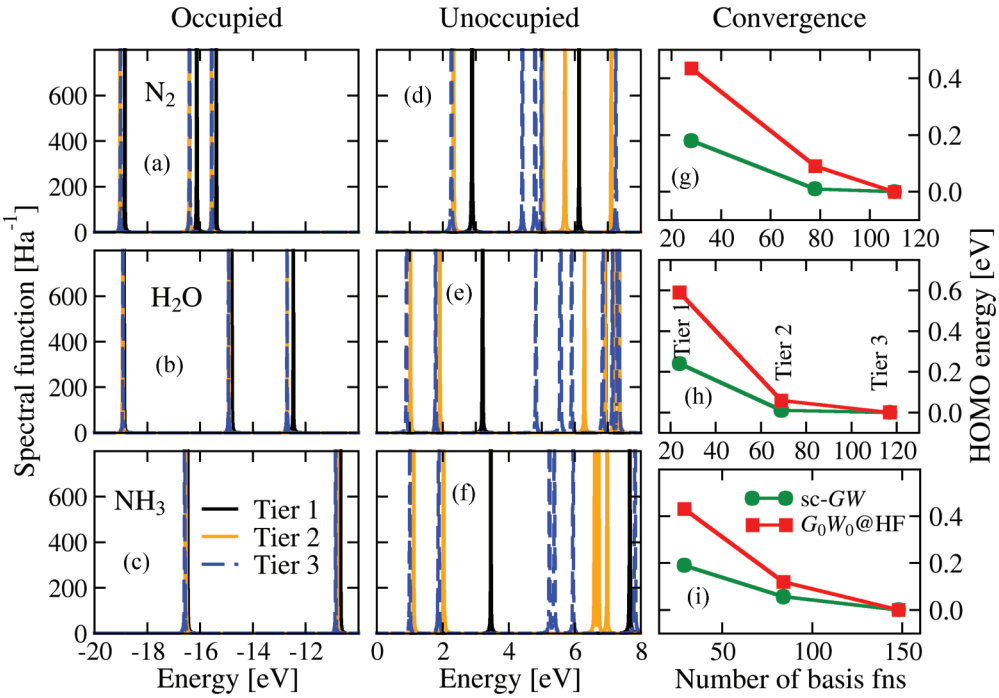


FIG. 6. (Color online) Spectral function calculated from Eq. (27) using a sc-$GW$ Green's function for $H_2O$, $NH_3$, and $N_2$ with Tier 1 (black line), Tier 2 (orange line), and Tier 3 (blue dashed line) NAO basis sets. Panels (a), (b), and (c) show the peaks corresponding to the first valence states; peaks relative to conduction states are reported in panels (d), (e), and (f). Finally, panels (g), (h), and (i) report the convergence of the highest occupied molecular orbital (HOMO) level as a function of the number of numerical orbitals used in the basis set.

to Tier 2. For $N_2$, for example, we observe a change in the highest occupied molecular orbital (HOMO) of approximately 0.2 eV going from Tier 1 (which consists of 14 NAO basis functions per atom) to Tier 2 (39 NAO per atom). A further increase of the basis set from Tier 2 to Tier 3 (55 NAO per atom) leads to changes of the order of 5 meV in the HOMO, as illustrated in the right panels of Fig. 6. Lower lying quasiparticle peaks show a similar convergence behavior as the HOMO. $H_2O$ and $NH_3$ exhibit a qualitatively similar behavior. Surprisingly, for all systems considered here, sc-$GW$ data converge faster with the basis set size than perturbative $G_0W_0$ calculations. In the following, we focus on closed-shell molecules, which in many instances do not have a stable anionic state. Therefore, we focus on the spectral function of occupied states only.

To investigate the performance of the $GW$ approximation at self-consistency, we have performed sc-$GW$ calculations for a set of molecules relevant for organic photovoltaic applications. We report in Fig. 7 the comparison between experimental[47–51] and theoretical ionization energies evaluated from sc-$GW$ and $G_0W_0$ based on the HF, PBE, and PBE0 starting points, for thiophene, benzothiazole, 1,2,5-thiadiazole, naphthalene, and tetrathiafulvalene. For an unbiased assessment, it would be desirable to benchmark sc-$GW$ against higher level theories, since in experiment the distinction between vertical and adiabatic ionization energies is difficult and vibrational effects are always present. For naphthalene the coupled-cluster singles doubles with perturbative triples [CCSD(T)] method, which is currently considered as the gold standard in quantum chemistry, gives a vertical ionization potential of 8.241 eV,[52] which sc-$GW$ underestimates (7.48 eV). For this molecule, the difference between the vertical and the adiabatic ionization potential is only 0.1 eV in CCSD(T). For thiophene, CCSD(T) calculations of the adiabatic ionization energy obtain 8.888 eV,[53] in good agreement with experiment, whereas sc-$GW$ yields 8.45 eV. Zero-point vibration effects are small and cancel with core-correlation and relativistic effects. However, the authors of this study indicate that the geometry of the cation differs considerably from that of the molecule, but did not give values for the vertical ionization energy. Therefore, it remains open to which degree the vertical and adiabatic ionization potentials of thiophen differ. For benzothiazole, 1,2,5-thiadiazole, and tetrathiafulvalene we were not able to find CCSD(T) calculations for the vertical ionization potential.

Despite the tendency to underestimate the first ionization energy, for these systems sc-$GW$ ionization energies are in good agreement with experiment, and give a good overall description of the excitation spectrum: full self-consistency leads to an average error of 0.4 eV (with a maximum error of 1.2 eV) between the experimental and theoretical ionization energies, whereas HF- and PBE-based $G_0W_0$ differs, on average, by 0.7 eV (with a maximum error of 1.5 eV for $G_0W_0$@HF, and 1.6 eV for $G_0W_0$@PBE). Interestingly, $G_0W_0$@PBE0 ionization energies are close to the sc-$GW$ ones. Moreover, the $G_0W_0$@PBE0 spectrum is in slightly better agreement with experiment with an average deviation of 0.3 eV (with a maximum error of 1.2 eV), as recently also reported for benzene and the azabenzenes in Ref. 12.

For small molecules, the improvements of the spectral properties at self-consistency can partially be traced back to corrections of the over- or underscreening in $G_0W_0$. In PBE based $G_0W_0$ calculations, the small HOMO-LUMO (lowest unoccupied molecular orbital) gap induces an overestimation

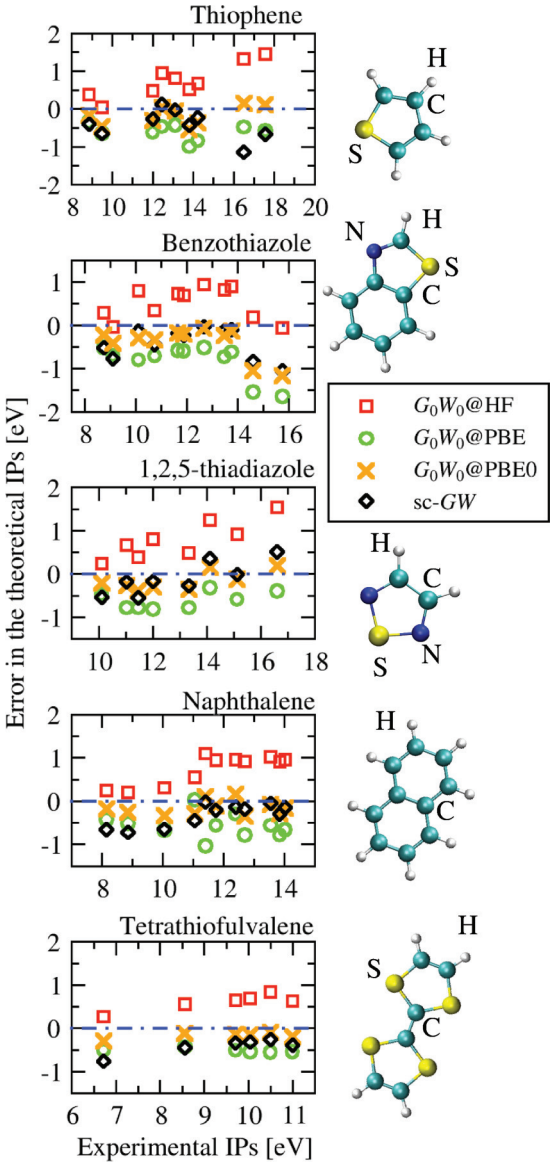


FIG. 7. (Color online) Comparison between theoretical and experimental vertical ionization energies of thiophene, benzothiazole, 1,2,5−thiadiazole, naphthalene, and tetrathiafulvalene. Experimental photoemission data are from Refs. 47–51. The molecular geometries were optimized with PBE in a Tier 2 basis set and are reported on the right. $G_0W_0$ ionization energies are obtained with a Tier 4 basis set, the sc-$GW$ ones with a Tier 2 basis.

of the screening in the Coulomb interaction. This is the origin of a systematic error in the $G_0W_0$@PBE quasiparticle energies. Similar considerations are easily generalized to the HF starting point, where HOMO-LUMO gaps are generally too large due to the missing correlation energy. PBE0, on the other hand, often gives a good compromise. Therefore, the over- and underscreening is reduced in $G_0W_0$@PBE0 and the resulting excitation spectrum is similar to sc-$GW$, where—because of the self-consistent calculation of $W$—this problem is mitigated. Based on these results, PBE0 emerges as an optimal starting point for the perturbative calculation of the spectral properties. It was argued that the screened Coulomb interaction obtained from sc-$GW$ may also be underscreened due to the lack of electron-hole interactions, typically accounted for by vertex corrections.[54] This would, in principle, lead to a systematic overestimation of the quasiparticle energies, as reported in Ref. 55 for semiconductors. Figure 7, on the other hand, indicates a slight underestimation of the sc-$GW$ quasiparticle energies, confirming the expectation that effects of the electron-hole attraction on the screened Coulomb interaction are small in molecules with large HOMO-LUMO gaps.

As alluded to in the Introduction, previous sc-$GW$ studies have reported conflicting conclusions on the accuracy of the spectral properties.[9,18–20,25] Consequently, no consensus has so far been reached in this respect. sc-$GW$ calculations for the HEG indicated a deterioration of the spectra as compared to perturbative $G_0W_0$ based on the local-density approximation (LDA).[18] For the HEG, Holm and von Barth observed a transfer of spectral weight from the plasmon satellite to the quasiparticle peak in self-consistent calculations.[18] This results in a weaker plasmon peak and a broader valence band, which worsens the agreement with photoemission experiments for metallic sodium.

The first self-consistent calculation for real systems—performed for potassium and silicon in the pseudopotential approximation—confirmed the picture outlined by Holm and von Barth, indicating a deterioration of the bandwidth and band gap at self-consistency.[19] In a later work, Ku and Eguiluz attributed the origin of this failure to the pseudopotential approximation, emphasizing the importance of accounting for core-valence coupling in the determination of the screening.[20] However, several groups[23,56,57] have questioned the convergence of these calculations with respect to the number of bands. Nevertheless, these earlier studies gave the impression that full self-consistency deteriorates the spectral properties compared to perturbative $G_0W_0$, and that it is not recommended to perform sc-$GW$ calculations. However, in our opinion, the scarce numerical evidence for realistic systems is not enough to corroborate this notion.

It was argued that the deterioration of spectra in sc-$GW$ might arise due to the iterative construction of the polarizability $\chi$ as the product of two Green's functions.[43] This would systematically weaken the incoherent part of the Green's function and reduce the intensity of the plasmon satellites. For molecules, however, this mechanism does not apply since quasiparticle peaks carry integer spectral weight, and no plasmon satellites are observed. For extended systems, this mechanism might effectively deteriorate the sc-$GW$ spectral function, as for the HEG. Nonetheless, more investigations are needed to provide a general and systematic assessment of sc-$GW$ for real solids.

### A. Lifetimes of quasiparticle peaks

To facilitate the comparison between $G_0W_0$@PBE0 and sc-$GW$, we report in Fig. 8 the full sc-$GW$ and $G_0W_0$@PBE0 spectral function of thiophene and 1,2,5-thiadiazole. Figure 8 illustrates that even if the peak positions in sc-$GW$ and $G_0W_0$@PBE0 are very similar, there are qualitative differences.

We observe that quasiparticle peaks corresponding to high-energy excitations are accompanied by a finite broadening. The

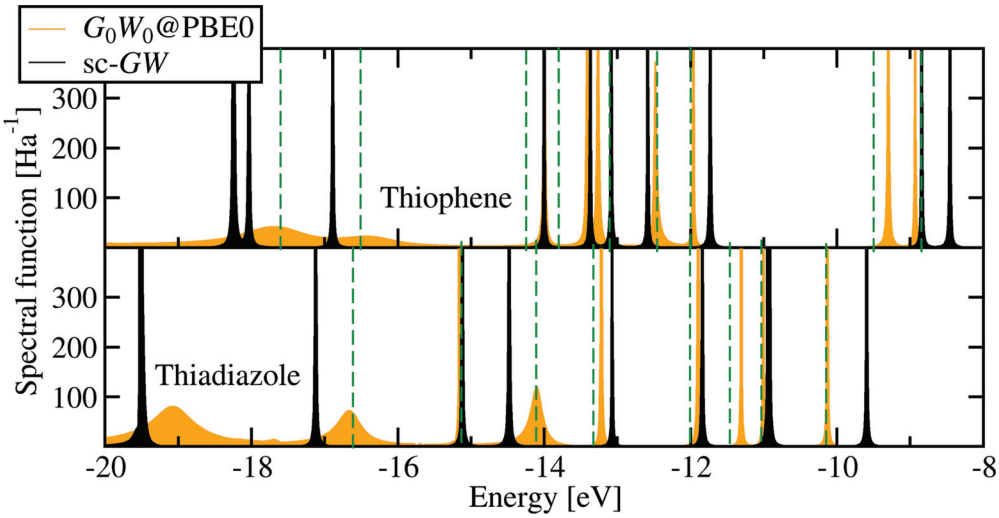


FIG. 8. (Color online) Comparison between sc-$GW$ and $G_0W_0$@PBE0 spectral functions for thiophene and 1,2,5-thiadiazole evaluated with a Tier 2 basis set. Vertical dashed lines indicates experimental photoemission data from Refs. 47 and 48, respectively. $G_0W_0$@PBE0 spectra are obtained with a Tier 4 basis set, and the sc-$GW$ spectra are obtained with a Tier 2 basis.

broadening in turn, being inversely proportional to the lifetime of the corresponding quasiparticle state, yields important information on the dynamics and damping of excitations. In finite systems, finite lifetimes of electronic excitations are a well-known aspect that has been extensively discussed in the literature. For single atoms, for which vibrational decay channels are not available, electronic lifetimes of holes have been measured with photoemission[58] and pump-probe techniques.[59] The most likely process that leads to the decay of holes is Auger recombination.

Green's function theory is, in principle, exact, and is therefore expected to correctly account for the lifetime (i.e., the broadening) of quasiparticle excitations if the exact self-energy were used. The origin of peak broadening can easily be understood from the structure of the Lehmann representation,

$$G^{\sigma}(\mathbf{r},\mathbf{r}',\omega) = \sum_{s} \frac{f_s^{\sigma}(\mathbf{r}) f_s^{*\sigma}(\mathbf{r}')}{\omega - \varepsilon_s - i\eta}, \tag{29}$$

where we considered only holes for simplicity. $f_s$ are the Lehmann amplitudes and the energies are defined as $\varepsilon_s \equiv E_s^{N-1} - E_0^N$, where $E_0^N$ denotes the ground-state energy of the $N$-particle system. $E_s^{N-1}$ are the excited-state energies of the $N$-1 particle system (i.e., they solve $\hat{H}\Psi_s^{N-1} = E_s^{N-1}\Psi_s^{N-1}$, where $\hat{H}$ is the many-body Hamiltonian). Typically, such a neutral excitation spectrum exhibits a few discrete peaks, if the $N$-1 particle system has bound states, followed by a continuum as electrons are excited above the vacuum level. Therefore, if the hole left behind by the photoemission process is close to the Fermi energy, the energies $E_s^{N-1}$ (and subsequently also $\varepsilon_s$) are discrete. The spectral function therefore exhibits a series of $\delta$ functions. However, if the holes are low enough in energy, $E_s^{N-1}$ lies in the continuum of the $N$-1 particle systems. This is typically when $E_s^{N-1} - E_0^{N-1}$ is larger than the next ionization energy $E_0^{N-2} - E_0^{N-1}$, where $E_0^{N-2}$ and $E_0^{N-1}$ are the ground-state energies of the $N$-2 and $N$-1 particle systems, respectively. Correspondingly, $\varepsilon_s$ varies continuously and gives rise to a series of $\delta$ peaks that are infinitely closely spaced and merge into a single quasiparticle peak with a finite broadening.

For a quantitative assessment of lifetimes in molecules we would have to consider effects beyond $GW$, such as the coupling to vibrations and the satisfaction of selection rules in the decay process. However, this goes beyond the purpose of the present work. We therefore limit the following discussion to the origin of lifetimes in molecules and briefly characterize their starting point dependence.

For all molecules considered in this work, the quasiparticle peaks close to the Fermi energy have a $\delta$-function-like character. This structure reflects the infinite lifetime of the quasiparticle excitation and is due to the absence of allowed electronic transitions that could annihilate the hole created in the photoemission process. The excitations of lower valence and core electrons, on the other hand, may have a finite lifetime, and the quasiparticle peak gets broadened. The physical origin of the lifetime is simple. The hole created in a lower valence (or core) state by the photoemission process can, in principle, recombine with electrons close to the Fermi energy. The energy released in this process has to be converted into an internal excitation of the system, since isolated molecules cannot dissipate energy. If the energy released is larger than the HOMO-LUMO gap, a particle-hole pair can be created. This opens up a scattering or decay channel for the hole, which therefore acquires a lifetime. The energy threshold for electron-hole formation is then given by $\Delta \equiv E_{\mathrm{HOMO}}^{\mathrm{GS}} - E_{\mathrm{gap}}^{\mathrm{GS}}$, with $E_{\mathrm{HOMO}}^{\mathrm{GS}}$ and $E_{\mathrm{gap}}^{\mathrm{GS}}$ the HOMO level and the HOMO-LUMO gap of the starting point, respectively. In other words, only quasiparticle states with an energy below $\Delta$ may decay and acquire a finite broadening. This argument is general and does not only apply to $GW$. What is particular to $G_0W_0$ is that the relevant gap for this process is determined by the starting point; in this case the DFT functional for the ground state.

To illustrate this effect on the broadening of the quasiparticle peaks, we report in Fig. 9 the spectrum of benzene evaluated from $G_0W_0$ based on different starting points and at self-consistency. Values of $\Delta$ for the different exchange-correlation

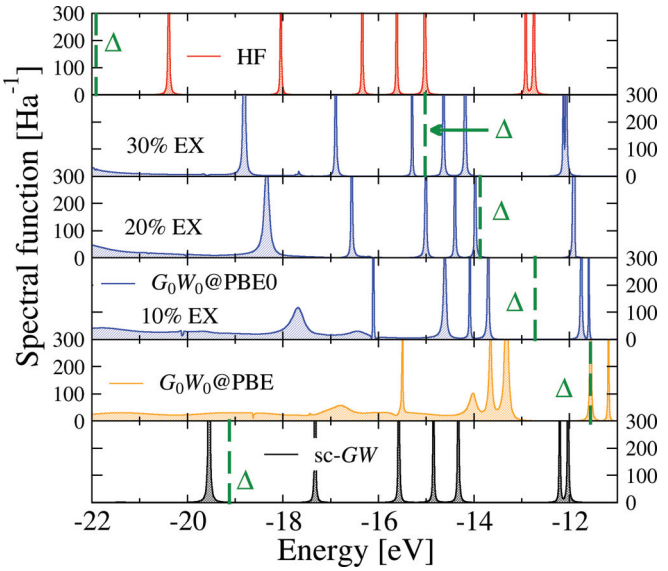


FIG. 9. (Color online) Spectral function of benzene evaluated from sc-$GW$ and $G_0W_0$ based on PBE, PBE0 with different mixture of exact exchange (EX) and HF. Vertical dashed lines (in green) indicate the energy threshold $\Delta$ for the formation of an electron-hole pair, which depends explicitly on the HOMO and LUMO levels of the underlying DFT/HF calculation. The quasiparticle peaks acquire a finite broadening only for states below $\Delta$. For peaks above $\Delta$, the residual broadening stems from the parameter $\eta = 10^{-4}$ discussed in the text.

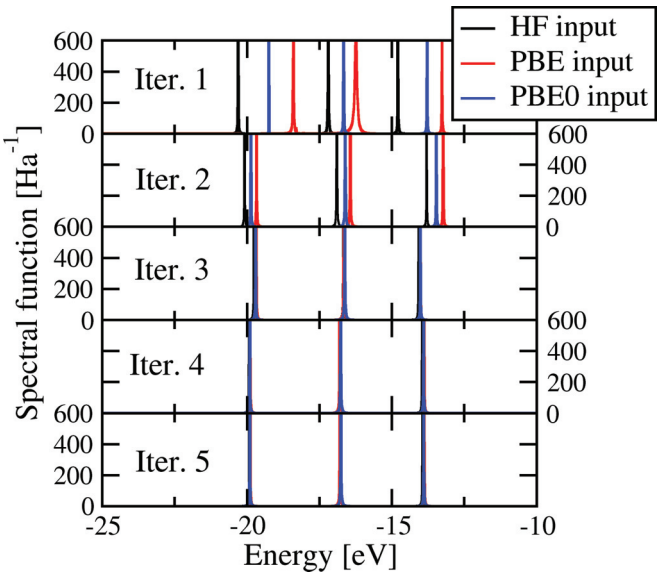


FIG. 10. (Color online) Spectral function of the CO dimer evaluated for the first five iterations of the Dyson equation from the HF, PBE, and hybrid PBE0 starting points. The first iteration corresponds to the $G_0W_0$ approximation.

functionals are reported as vertical dashed lines (in green). PBE has the smallest HOMO-LUMO gap (∼5.2 eV) and we observe a noticeable peak broadening (i.e., short lifetime) at ∼14 eV in the $G_0W_0$@PBE spectrum. A systematic increase of the broadening is then observed the further a state lies below $\Delta$. Adding exact exchange to the DFT functional and increasing its admixture opens the HOMO-LUMO gap. The onset of the finite lifetime subsequently moves to lower energies.

In sc-$GW$, the broadening of the quasiparticle peaks is consistent with the HOMO-LUMO gap at the $GW$ level, and the ambiguity of the starting point dependence is lifted. Consequently, for benzene only peaks below −19 eV acquire a small finite broadening. Based on the sc-$GW$ results, the large broadening observed in the $G_0W_0$@PBE0 spectrum can be attributed to the small HOMO-LUMO gap of the underlying PBE0 calculation. The inclusion of a fraction of exact exchange partially ameliorates this problem, but not fully. This indicates that the calculation of lifetimes presents an additional situation in which—due to the severe dependence on the starting point—resorting to full self-consistency is essential.

### B. Independence of the starting point

Previous work showed that partially self-consistent approaches such as eigenvalue self-consistent $GW$[10] or quasiparticle self-consistency,[43,44] reduce the starting-point dependence but they do not eliminate it.[12,60] Only full self-consistency successfully removes any dependence on the starting point, as we discussed in Ref. 17. This is a major advantage of the sc-$GW$ scheme, as it allows a systematic assessment of the $GW$ approximation unbiased by a spurious dependence on the input Green's function.

To illustrate the independence of the starting point of the sc-$GW$ Green's function, we report in Fig. 10 the spectral function of the carbon monoxide molecule as a function of the number of iterations of the Dyson equation initialized with HF, PBE, and PBE0. After just a few iterations of the sc-$GW$ loop, the quasiparticle peaks in the spectral function are located at the same energies, demonstrating the independence of the starting point in sc-$GW$.

## V. GROUND-STATE PROPERTIES FROM THE $GW$ APPROXIMATION

### A. Galitskii-Migdal total energy

In MBPT, the total energy $E_{\rm tot}$ may be regarded as an explicit functional of the Green's function, i.e., $E_{\rm tot} = E_{\rm tot}[G]$. The functional dependence of $E_{\rm tot}[G]$ on $G$ is not uniquely defined and different total energy functionals have been proposed over the years. Some examples are the Luttinger-Ward[61] and the Klein functional[62]—which are stationary at the self-consistent Green's function[63]—and the Galitskii-Migdal formula.[64] The total energy obtained from different functionals may differ in principle, if evaluated with a given Green's function. However, if the Green's function is obtained self-consistently solving the Dyson equation, all functionals yield the same, unique total energy. Since we are interested in sc-$GW$ total energies, all total energy functionals are equivalent and we use the Galitskii-Migdal formula because of its simplicity:

$$E_{\rm GM} = -i \int \sum_{\sigma} \frac{d\omega}{2\pi} Tr\{[\omega + h_0] G^{\sigma}(\omega)\} + E_{\rm ion}. \qquad (30)$$

Here $h_0$ is the single-particle term of the many-body Hamiltonian, i.e., the sum of the external potential due to the

nuclei and the kinetic energy operator, and $E_{\rm ion}$ accounts for the repulsive nuclear energy. As discussed in Ref. 32, Eq. (30) can be computed directly in imaginary frequency taking advantage of the reduced size of the integration grid needed to describe $G$ and $\Sigma$ on the imaginary axis. In the present work, we cast Eq. (30) into a more suitable form for numerical implementations,[65]

$$E_{\rm GM} = -i\sum_{ij,\sigma}\overline{G}^{\sigma}_{ij}(\tau=0^-)\left[2t_{ji}+2v^{\rm ext}_{ji}+v^{\rm H}_{ji}+\Sigma^{\rm x}_{ji,\sigma}\right] - i\sum_{ij,\sigma}\int\frac{d\omega}{2\pi}\overline{G}^{\sigma}_{ij}(\omega)\Sigma^{\rm c}_{ji,\sigma}(\omega)e^{i\omega\eta}+E_{\rm ion}, \qquad (31)$$

where $t$ denotes the kinetic-energy operator, $v^{\rm H}$ and $v^{\rm ext}$ the Hartree and external potential, and $\Sigma^{\rm x}$ and $\Sigma^{\rm c}$ the exchange and correlation parts of the self-energy, respectively. We used $\overline{G}\equiv s^{-1}Gs^{-1}$, with $s_{ij}=\int d\mathbf{r}\varphi_i(\mathbf{r})\varphi_j(\mathbf{r})$. A derivation of Eq. (31) is reported in Appendix A. We emphasize that Eq. (31) is exact if evaluated with the exact self-energy and Green's function. In Eq. (31) contributions arising from time-independent operators can be easily evaluated by simple matrix products. The correlation energy, on the other hand, requires a frequency integration which can be evaluated directly on the imaginary frequency axis without resorting to the analytic continuation.[32] We evaluated Eq. (31) in the $GW$ approximation. In sc-$GW$, both $\Sigma$ and $G$ are self-consistent solution of the Dyson equation, whereas for $G_0W_0$ the self-energy is evaluated only once and $G$ is the noninteracting Green's function of the DFT/HF calculation. The latter procedure corresponds to a first-order perturbative correction of the DFT/HF total energy, with a perturbing potential given by $[\Sigma(\omega)-v_{\rm xc}]$.

### B. Structural parameters of diatomic molecules

Total energy differences are more important than absolute total energies, as they give information on structural properties and on the strength of chemical bonds. Here, we restrict the discussion to the ground-state properties of dimers at their equilibrium geometry. The reader is referred to Ref. 66 for an assessment of the sc-$GW$ method in the dissociation limit.

In the following, we provide an assessment of the sc-$GW$ method for bond lengths, binding energies, and vibrational frequencies based on the calculations of the potential energy curve of LiH, LiF, HF, CO, $H_2$, and $N_2$. To illustrate the convergence with the basis set, we report in Fig. 11 the binding energy of the carbon monoxide dimer evaluated with sc-$GW$, RPA@PBE, $G_0W_0$@PBE, and PBE-based renormalized second-order perturbation theory[67,68] (rPT2) using increasingly larger NAO basis sets (Tiers 1–4).

The MAEs of theoretical bond lengths, binding energies, and vibrational frequencies as compared to experiment are reported in Fig. 12. The corresponding numerical values are reported in Appendix B. Since our calculations are performed in the Born-Oppenheimer approximation with clamped nuclei, we compared our calculations with zero-point motion corrected experimental binding energies from Ref. 69. PBE, HF, and several perturbative approaches based on MBPT, namely $G_0W_0$, EX + cRPA, and rPT2 are included for comparison.

Self-consistency provides better bond lengths than perturbative $G_0W_0$ calculations. However, the accuracy achieved by

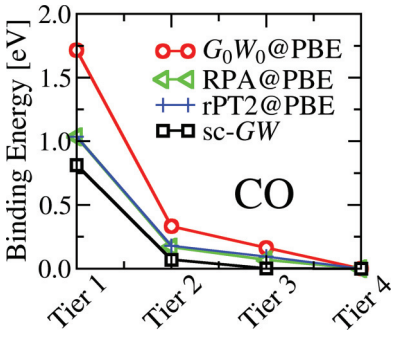


FIG. 11. (Color online) BSSE corrected binding energy of CO evaluated with Tiers 1, 2, 3, and 4. Each curve is aligned at their respective Tier 4 value. All data are in eV.

sc-$GW$ for the bond lengths is still comparable to perturbative RPA and not as good as rPT2@PBE, which includes higher order exchange and correlation diagrams.

The binding energies obtained from $G_0W_0$ based on HF and PBE, reported in Table II, are systematically overestimated. Self-consistent $GW$ overcorrects this trend and yields binding energies that slightly underestimate experiment. RPA@HF and sc-$GW$ give a very similar description of the binding energy, the deviation between the two methods being approximately 10–20 meV. This similarity is expected for two reasons. First,

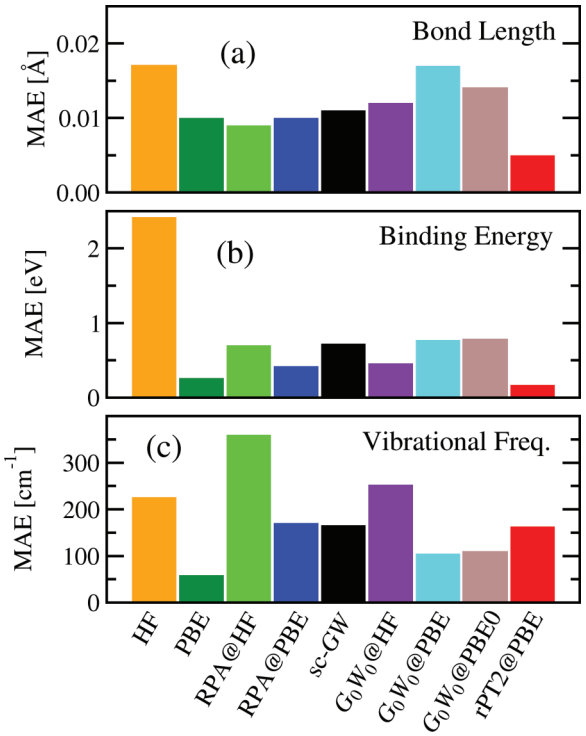


FIG. 12. (Color online) Mean absolute error (MAE) of bond lengths (top panel), binding energies (middle panel), and vibrational frequencies (bottom panel) of LiH, LiF, HF, CO, $H_2$, and $N_2$ evaluated at different levels of theory. The estimated zero-point motion correction has been subtracted from the experimental binding energies (reported from Ref. 69). Calculations were done with a Tier 3 basis set (the largest basis set available) for $H_2$, LiH, and HF, whereas a Tier 4 basis was used for $N_2$ and CO. Numerical values are reported in Tables II, III, and IV in Appendix B.

in diatomic molecules screening is small; thus, the sc-$GW$ Green's function resembles the HF one (since in absence of polarization $W$ reduces to the bare Coulomb interaction). Second, the RPA total energy is a variational functional of the Green's function, and therefore RPA total energies are close to sc-$GW$ ones, if the input Green's function is *close enough* to the sc-$GW$ Green's function.[16] Larger discrepancies between perturbative RPA and sc-$GW$ are to be expected for the structural properties of systems for which the sc-$GW$ density is substantially different as compared to HF or semilocal DFT. Examples of these material are molecular interfaces and charge transfer compounds, where the ground-state density (and the charge transfer) depends strongly on the level alignment between the individual components of the system. This will be addressed in future works. Also, for binding energies and bond lengths, sc-$GW$ is outperformed by rPT2@PBE, which illustrates the importance of including exchange and correlation diagrams beyond the $GW$ approximation for a systematic improvement of the ground-state properties of finite systems.

For vibrational frequencies, the dependence on the starting point is larger than for binding energies or bond lengths. In this case, the best agreement with experiment is achieved with the PBE functional, whereas for HF the errors are substantially larger. Similarly, PBE-based $G_0W_0$ and EX + cRPA deviate less from experiment than HF-based schemes. For instance, the MAE of EX + cRPA@HF is approximately a factor of two larger than EX + cRPA@PBE, and the same is observed for $G_0W_0$. Consequently, sc-$GW$ gives smaller MAEs compared to HF-based schemes, but does not improve over PBE-based perturbative schemes.

### C. Density and dipole moments at self-consistency

In perturbative approaches, such as $G_0W_0$, EX + cRPA, and rPT2, the electron density of a system is defined by the eigenstates of the unperturbed reference Hamiltonian, although in principle perturbative corrections to the eigenstates of the unperturbed Hamiltonian could be calculated. This constitutes a major drawback, as it is, in part, responsible for the well-known starting point dependence of perturbative schemes. Self-consistency, on the other hand, permits us to incorporate exact exchange and dynamical correlation effects into the electron density. To illustrate this aspect in sc-$GW$, we discuss in the following the effects of self-consistency on the density and the dipole moment of diatomic molecules.

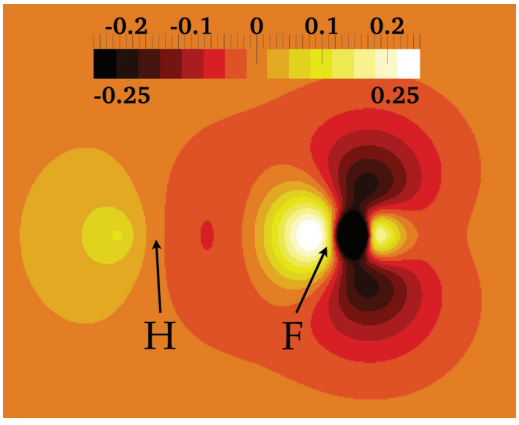


FIG. 13. (Color online) Difference between the sc-$GW$ and HF densities for the hydrogen fluoride dimer at its experimental equilibrium geometry ($d = 0.917$ Å). At self-consistency, electron density is shifted from negative (dark) to positive regions (light). Units are Å$^{-3}$ and the calculation were performed using a Tier 3 basis set.

TABLE I. Comparison between experimental[70] and theoretical dipole moments evaluated from sc-$GW$, PBE, and HF at their corresponding equilibrium bond lengths. All values are in Debye.

| | LiH | HF | LiF | CO | MAE |
|---|---|---|---|---|---|
| Exp. | 5.88 | 1.82 | 6.28 | 0.11 | |
| sc-$GW$ | 5.90 | 1.85 | 6.48 | 0.07 | 0.07 |
| PBE | 5.63 | 1.77 | 6.12 | 0.20 | 0.14 |
| PBE0 | 5.77 | 1.81 | 6.20 | 0.09 | 0.06 |
| HF | 6.04 | 1.89 | 6.46 | −0.13 | 0.17 |

Figure 13 shows the density difference between sc-$GW$ and HF for the hydrogen fluoride dimer. The density difference illustrates the effects of $GW$ correlation on the electron density. sc-$GW$ enhances the angular distribution of the electron density exhibiting more pronounced angular correlation. Moreover, density is shifted from the two lobes perpendicular to the molecular axis to the bond region, leading to a reduction of the dipole moment as compared to HF, which is in better agreement with experiment (see Table I).

The dipole moment provides a systematic way to quantify the quality of the electron density of a system, as it is directly comparable with experimental data. We report in Table I the dipole moment of LiH, LiF, HF, and CO evaluated from sc-$GW$, PBE, and HF. sc-$GW$ dipole moments are in good agreement with experiments and reduce the deviation from experiment by approximately a factor of two compared to HF and PBE, that tend to under- and overestimate, respectively. The quality of the dipole moment for the small set of molecules presented here, indicates that sc-$GW$ is a promising method for the description of charge-trasfer compounds, such as molecular interfaces and heterostructures.

## VI. CONCLUSIONS

We have presented an all-electron implementation of the *fully* self-consistent $GW$ method based on a NAO basis in the FHI-AIMS code.[27] Self-consistent $GW$ is based on the iterative solution of Hedin's equations with the $GW$ self-energy and polarizability, and therefore it is significantly different from partially self-consistent approaches based on perturbation theory, such as the quasiparticle self-consistent $GW$ scheme[43,44] and self-consistency in the eigenvalues.[10,71]

In our implementation, the two-particle operators are treated efficiently by means of the resolution of identity technique.[31] The introduction of an auxiliary basis for the representation of the frequency and time dependence of dynamic operators facilitates an accurate evaluation of Fourier integrals that require just few tens of grid points. These ingredients allow us to reformulate Hedin's equations in a matrix form, which can be solved with standard linear algebra packages.

We presented an assessment of the spectral properties of five molecules of interest for organic photovoltaic applications:

thiophene, benzothiazole, 1,2,5-thiadiazole, naphthalene, and tetrathiafulvalene. For these systems, the quasiparticle energies extracted from the sc-$GW$ spectral function are found to be in good agreement with experimental photoemission data for all valence states. The sc-$GW$ excitation spectrum systematically improves over perturbative $G_0W_0$ based on semilocal DFT and HF. This is interpreted as a consequence of the mitigation of over- and underscreening errors characteristic of $G_0W_0$@PBE and $G_0W_0$@HF, respectively. $G_0W_0$ based on PBE0, on the other hand, provides results in slightly better agreement with experimental data than sc-$GW$. Thus, the PBE0 functional appears to be close to an optimal starting point for perturbative calculations.

Self-consistent $GW$ total energies based on the Galitskii-Migdal formula permit an assessment of ground-state and structural properties of molecules. For a small set of diatomic molecules we evaluated binding energies, bond lengths, and vibrational frequencies. The bond lengths improve at self-consistency, but still have an accuracy comparable to other perturbative methods such as exact exchange with correlation from the RPA. Binding energies are typically underestimated compared to experimental reference data and do not substantially improve over perturbative $G_0W_0$ calculations. Our results indicate and quantify the importance of including vertex corrections—or alternatively, higher order correlation and exchange diagrams—in order to achieve an accurate description of the structural properties of molecules.

Finally, the dipole moments of a set of heteroatomic dimers were studied to investigate the accuracy of the sc-$GW$ density. Compared to HF and PBE, the sc-$GW$ dipole moments are found in better agreement with experiment. These results indicate that sc-$GW$ is a promising approach for the description of charge-transfer compounds and heterojunctions, where the relative ordering of the frontier orbitals influences the charge transfer at the interface.

## ACKNOWLEDGMENTS

We would like to thank Christoph Friedrich for fruitful discussions. A.R. acknowledges financial support from the European Research Council Advanced Grant DYNamo (Grant No. ERC-2010-AdG-267374), Spanish Grants No. 2010-21282-C02-01 and No. PIB2010US-00652, Grupos Consolidados UPV/EHU del Gobierno Vasco (Grant No. IT578-13), and European Commission projects CRONOS (Grant No. 280879-2 CRONOS CP-FP7).

## APPENDIX A: REWRITING THE GALITSKII-MIGDAL FORMULA

In Hartree atomic units ($\hbar = e^2 = m = 1$), the electronic contribution of the Galitskii-Migdal total energy is[1]

$$E_{\mathrm{GM}} = -i \sum_{\sigma} \int d\mathbf{r}\, dt \lim_{\substack{\mathbf{r}'\to\mathbf{r} \\ t'\to t^+}} \left[ i\frac{\partial}{\partial t} + h_0 \right] G^{\sigma}(\mathbf{r}t,\mathbf{r}'t'). \quad \text{(A1)}$$

Here, $h_0$ is the single-particle term of the many-body Hamiltonian, i.e., the sum of the kinetic energy operator and the external potential due to the nuclei. Introducing the equation of motion for the interacting Green's function (see, e.g., Ref. 72),

$$\left[ i\frac{\partial}{\partial t} + \frac{\nabla_{\mathbf{r}}^2}{2} - v_{\mathrm{H}}(\mathbf{r}) - v_{\mathrm{ext}}(\mathbf{r}) \right] G^{\sigma}(\mathbf{r}t,\mathbf{r}'t') - \int d\mathbf{r}''dt''\, \Sigma^{\sigma}(\mathbf{r}t,\mathbf{r}''t'')G^{\sigma}(\mathbf{r}''t'',\mathbf{r}'t') = \delta(\mathbf{r}-\mathbf{r}')\delta(t-t'), \quad \text{(A2)}$$

Eq. (A1) can be simplified by eliminating the partial derivative with respect to time, obtaining

$$E_{\mathrm{GM}} = -i \sum_{\sigma} \int d\mathbf{r}\, d\mathbf{r}'dt\, dt' \lim_{\substack{\mathbf{r}'\to\mathbf{r} \\ t'\to t^+}} \left[ \left( -\nabla_{\mathbf{r}}^2 + 2v_{\mathrm{ext}}(\mathbf{r}) + v_{\mathrm{H}}(\mathbf{r}) \right) \times \delta(\mathbf{r}-\mathbf{r}')\delta(t-t') + \Sigma^{\sigma}(\mathbf{r}t,\mathbf{r}'t') \right] G^{\sigma}(\mathbf{r}'t',\mathbf{r}'t'). \quad \text{(A3)}$$

Making use of the matrix representation of the Green's function $G^{\sigma}(\mathbf{r},\mathbf{r}',\tau) = \sum_{ij} \varphi_i(\mathbf{r})\overline{G}^{\sigma}_{ij}(\tau)\varphi_j(\mathbf{r}')$—with $\overline{G}^{\sigma} \equiv s^{-1}G^{\sigma}s^{-1}$—the first three terms in Eq. (A3) can be rewritten as

$$\begin{aligned} -i \sum_{\sigma} \int d\mathbf{r} \lim_{\mathbf{r}'\to\mathbf{r}} \left[ -\nabla_{\mathbf{r}}^2 + 2v_{\mathrm{ext}}(\mathbf{r}) + v_{\mathrm{H}}(\mathbf{r}) \right] & \times \sum_{ij} \varphi_i(\mathbf{r})\overline{G}^{\sigma}_{ij}(\tau = 0^-)\varphi_j(\mathbf{r}') \\ &= -i \sum_{\sigma} \sum_{ij} \overline{G}^{\sigma}_{ij}(\tau = 0^-)\left[ 2t_{ji} + 2v^{\mathrm{ext}}_{ji} + v^{\mathrm{H}}_{ji} \right]. \end{aligned} \quad \text{(A4)}$$

For time-independent Hamiltonians, the Green's function depends only on time differences $\tau \equiv t - t'$. In the last step of Eq. (A4), we defined the matrix representation of the kinetic energy operator as $t_{ij} = \int d\mathbf{r}\varphi_i(\mathbf{r})[-\frac{\nabla_{\mathbf{r}}^2}{2}]\varphi_j(\mathbf{r})$, and use a similar representation for $v^{\mathrm{ext}}_{ji}$ and $v^{\mathrm{H}}_{ji}$. Finally, the last term in Eq. (A3) can be rearranged by using the

TABLE II. sc-$GW$ and perturbative $G_0W_0$ binding energies (evaluated from the Galitskii-Migdal formula) of diatomic molecules compared to (zero-point motion corrected) experimental reference data taken from Ref. 69. We report perturbative RPA, HF, PBE, and renormalized second-order perturbation theory (rPT2) for comparison. Calculations were done with a Tier 3 basis set (the largest basis set available) for $H_2$, LiH, and HF, whereas a Tier 4 basis was used for $N_2$ and CO. The mean absolute errors (MAE) are reported in panel (b) of Fig. 12. All values are in eV.

| | $H_2$ | LiH | HF | LiF | $N_2$ | CO | MAE |
|---|---|---|---|---|---|---|---|
| Exp | −4.75 | −2.52 | −6.12 | −6.02 | −9.91 | −11.24 | |
| sc-$GW$ | −4.41 | −2.16 | −5.55 | −5.50 | −8.42 | −10.19 | 0.72 |
| $G_0W_0$@HF | −5.05 | −2.72 | −6.45 | −6.60 | −10.61 | −11.88 | 0.46 |
| $G_0W_0$@PBE | −5.44 | −2.94 | −6.46 | −6.37 | −11.82 | −12.16 | 0.77 |
| $G_0W_0$@PBE0 | −5.32 | −2.90 | −6.49 | −6.67 | −11.50 | −12.34 | 0.78 |
| RPA@HF | −4.41 | −2.17 | −5.54 | −5.52 | −8.51 | −10.19 | 0.70 |
| RPA@PBE | −4.68 | −2.32 | −5.60 | −5.43 | −9.54 | −10.48 | 0.42 |
| rPT2@PBE | −4.71 | −2.49 | −5.93 | −5.90 | −9.42 | −11.06 | 0.72 |
| HF | −3.64 | −1.49 | −4.22 | −3.95 | −5.10 | −7.62 | 2.42 |
| PBE | −4.54 | −2.32 | −6.17 | −6.03 | −10.58 | −11.67 | 0.26 |

TABLE III. sc-$GW$ and perturbative $G_0W_0$ bond lengths of diatomic molecules compared to experimental reference data taken from Ref. 70. RPA, HF, PBE, and renormalized second-order perturbation theory (rPT2) are included for comparison. Mean absolute errors (MAE) are reported in panel (a) of Fig. 12. All values are in Å.

| | $H_2$ | LiH | HF | LiF | $N_2$ | CO | MAE |
|---|---|---|---|---|---|---|---|
| Exp. | 0.741 | 1.595 | 0.917 | 1.564 | 1.098 | 1.128 | |
| sc-$GW$ | 0.735 | 1.579 | 0.919 | 1.586 | 1.085 | 1.118 | 0.011 |
| $G_0W_0$@HF | 0.733 | 1.560 | 0.919 | 1.579 | 1.093 | 1.119 | 0.012 |
| $G_0W_0$@PBE | 0.746 | 1.582 | 0.938 | 1.593 | 1.116 | 1.143 | 0.017 |
| $G_0W_0$@PBE0 | 0.741 | 1.564 | 0.932 | 1.590 | 1.100 | 1.136 | 0.014 |
| RPA@HF | 0.734 | 1.587 | 0.914 | 1.576 | 1.087 | 1.117 | 0.009 |
| RPA@PBE | 0.745 | 1.597 | 0.927 | 1.589 | 1.107 | 1.137 | 0.010 |
| rPT2@PBE | 0.739 | 1.597 | 0.914 | 1.578 | 1.091 | 1.125 | 0.005 |
| HF | 0.734 | 1.606 | 0.898 | 1.560 | 1.066 | 1.102 | 0.017 |
| PBE | 0.751 | 1.605 | 0.930 | 1.575 | 1.104 | 1.136 | 0.010 |

Fourier transform of the Green's function and the self-energy $G(t,t') = \int_{-\infty}^{+\infty} \frac{d\omega}{2\pi} e^{-i\omega(t-t')} G(\omega)$ and substituting the matrix representation of $G$:

$$-i \sum_{\sigma} \int d\mathbf{r}\, d\mathbf{r}''dt\, dt'' \lim_{\substack{\mathbf{r}'\to\mathbf{r} \\ t'\to t^+}} \Sigma^{\sigma}(\mathbf{r}t,\mathbf{r}''t'')G^{\sigma}(\mathbf{r}''t'',\mathbf{r}'t')$$

$$= -i \sum_{\sigma} \sum_{ij} \int \frac{d\omega}{2\pi} \Sigma^{\sigma}_{ji}(\omega) G^{\sigma}_{ij}(\omega) e^{i\omega\eta}. \quad \text{(A5)}$$

Summing Eqs. (A4) and (A5) and separating the self-energy in its exchange and correlation components $\Sigma_{ij}(\omega) = \Sigma^{\mathrm{x}}_{ij} + \Sigma^{\mathrm{c}}_{ij}(\omega)$, one finally arrives at the expression reported in Eq. (31). We refer to Ref. 73, for a discussion on the evaluation of the Galitskii-Migdal formula on the imaginary frequency axis.

TABLE IV. sc-$GW$ and perturbative $G_0W_0$ vibrational frequencies of diatomic molecules compared to experimental reference data taken from Ref. 70. RPA, HF, PBE, and renormalized second-order perturbation theory (rPT2) are included for comparison. The mean absolute errors (MAE) are reported in panel (c) of Fig. 12. All values are in $\mathrm{cm}^{-1}$.

| | $H_2$ | LiH | HF | LiF | $N_2$ | CO | MAE |
|---|---|---|---|---|---|---|---|
| Exp. | 4401 | 1405 | 4138 | 911 | 2359 | 2170 | |
| sc-$GW$ | 4533 | 1743 | 4266 | 971 | 2543 | 2322 | 166 |
| $G_0W_0$@HF | 4585 | 1827 | 4341 | 1010 | 2490 | 2647 | 252 |
| $G_0W_0$@PBE | 4341 | 1743 | 4130 | 971 | 2346 | 2322 | 105 |
| $G_0W_0$@PBE0 | 4425 | 1813 | 4273 | 922 | 2386 | 2222 | 109 |
| RPA@HF | 4533 | 1685 | 5512 | 952 | 2544 | 2321 | 360 |
| RPA@PBE | 4357 | 1691 | 4757 | 933 | 2354 | 2115 | 172 |
| HF | 4567 | 1473 | 4569 | 949 | 2736 | 2448 | 226 |
| PBE | 4320 | 1364 | 3991 | 899 | 2328 | 2128 | 59 |
| rPT2@PBE | 4460 | 1605 | 4620 | 922 | 2507 | 2251 | 163 |

## APPENDIX B: BINDING ENERGIES, BOND LENGTHS, AND VIBRATIONAL FREQUENCIES OF DIATOMIC MOLECULES

In Tables II and III we report counterpoise-corrected[74] binding energies and bond lengths for $H_2$, LiH, LiF, HF, $N_2$, and CO. The corresponding vibrational frequencies are reported in Table IV. The sc-$GW$ results are compared with experimental values[69,70] and several perturbative approaches based on MBPT, namely $G_0W_0$, EX + cRPA, and rPT2@PBE.[67,68] HF and PBE are included for comparison.


[1] A. L. Fetter and J. D. Walecka, *Quantum Theory of Many-Particle Systems* (Dover, Mineola, NY, 2003).
[2] L. Hedin, Phys. Rev. **139**, A796 (1965).
[3] F. Aryasetiawan and O. Gunnarsson, Rep. Prog. Phys. **61**, 237 (1998).
[4] G. Onida, L. Reining, and A. Rubio, Rev. Mod. Phys. **74**, 601 (2002).
[5] L. Hedin and S. Lundqvist, Solid State Phys. **23**, 1 (1970).
[6] P. Rinke, A. Qteish, J. Neugebauer, and M. Scheffler, Phys. Status Solidi B **245**, 929 (2008).
[7] P. Rinke, A. Qteish, J. Neugebauer, C. Freysoldt, and M. Scheffler, New J. Phys. **7**, 126 (2005).
[8] X. Blase, C. Attaccalite, and V. Olevano, Phys. Rev. B **83**, 115103 (2011).
[9] C. Rostgaard, K. W. Jacobsen, and K. S. Thygesen, Phys. Rev. B **81**, 085103 (2010).
[10] M. S. Hybertsen and S. G. Louie, Phys. Rev. B **34**, 5390 (1986).
[11] F. Fuchs, J. Furthmüller, F. Bechstedt, M. Shishkin, and G. Kresse, Phys. Rev. B **76**, 115109 (2007).
[12] N. Marom, F. Caruso, X. Ren, O. T. Hofmann, T. Körzdörfer, J. R. Chelikowsky, A. Rubio, M. Scheffler, and P. Rinke, Phys. Rev. B **86**, 245127 (2012).
[13] F. Bruneval and M. A. L. Marques, J. Chem. Theory Comput. **9**, 324 (2013).
[14] G. Baym and L. P. Kadanoff, Phys. Rev. **124**, 287 (1961).
[15] G. Baym, Phys. Rev. **127**, 1391 (1962).
[16] N. E. Dahlen, R. van Leeuwen, and U. von Barth, Phys. Rev. A **73**, 012511 (2006).
[17] F. Caruso, P. Rinke, X. Ren, M. Scheffler, and A. Rubio, Phys. Rev. B **86**, 081102(R) (2012).
[18] B. Holm and U. von Barth, Phys. Rev. B **57**, 2108 (1998).
[19] W.-D. Schöne and A. G. Eguiluz, Phys. Rev. Lett. **81**, 1662 (1998).
[20] W. Ku and A. G. Eguiluz, Phys. Rev. Lett. **89**, 126401 (2002).
[21] A. Kutepov, S. Y. Savrasov, and G. Kotliar, Phys. Rev. B **80**, 041103 (2009).
[22] A. Kutepov, K. Haule, S. Y. Savrasov, and G. Kotliar, Phys. Rev. B **85**, 155129 (2012).
[23] C. Friedrich, A. Schindlmayr, S. Blügel, and T. Kotani, Phys. Rev. B **74**, 045104 (2006).
[24] R. Gomez-Abal, X. Li, M. Scheffler, and C. Ambrosch-Draxl, Phys. Rev. Lett. **101**, 106404 (2008).
[25] A. Stan, N. E. Dahlen, and R. van Leeuwen, J. Chem. Phys. **130**, 114105 (2009).

[26]M. Strange, C. Rostgaard, H. Häkkinen, and K. S. Thygesen, Phys. Rev. B **83**, 115108 (2011).
[27]V. Blum, R. Gehrke, F. Hanke, P. Havu, V. Havu, X. Ren, K. Reuter, and M. Scheffler, Comp. Phys. Commun. **180**, 2175 (2009).
[28]J. L. Whitten, J. Chem. Phys. **58**, 4496 (1973).
[29]B. I. Dunlap, J. W. D. Connolly, and J. R. Sabin, J. Chem. Phys. **71**, 3396 (1979).
[30]J. W. Mintmire, J. R. Sabin, and S. B. Trickey, Phys. Rev. B **26**, 1743 (1982).
[31]X. Ren, P. Rinke, V. Blum, J. Wieferink, A. Tkatchenko, S. Andrea, K. Reuter, V. Blum, and M. Scheffler, New J. Phys. **14**, 053020 (2012).
[32]P. García-González and R. W. Godby, Phys. Rev. Lett. **88**, 056406 (2002).
[33]P. Umari, G. Stenuit, and S. Baroni, Phys. Rev. B **79**, 201104 (2009).
[34]F. Bruneval and X. Gonze, Phys. Rev. B **78**, 085125 (2008).
[35]J. A. Berger, L. Reining, and F. Sottile, Phys. Rev. B **82**, 041103 (2010).
[36]F. Giustino, M. L. Cohen, and S. G. Louie, Phys. Rev. B **81**, 115105 (2010).
[37]M. Feyereisen, G. Fitzgerald, and A. Komornicki, Chem. Phys. Lett. **208**, 359 (1993).
[38]F. Weigend, M. Häser, H. Patzelt, and R. Ahlrichs, Chem. Phys. Lett. **294**, 143 (1998).
[39]F. Weigend, Phys. Chem. Chem. Phys. **4**, 4285 (2002).
[40]H. Eshuis, J. Yarkony, and F. Furche, J. Chem. Phys. **132**, 234114 (2010).
[41]C. Friedrich, A. Schindlmayr, and S. Blügel, Comp. Phys. Commun. **180**, 347 (2009).
[42]F. Aryasetiawan and O. Gunnarsson, Phys. Rev. B **49**, 16214 (1994).
[43]S. V. Faleev, M. van Schilfgaarde, and T. Kotani, Phys. Rev. Lett. **93**, 126406 (2004).
[44]M. van Schilfgaarde, T. Kotani, and S. Faleev, Phys. Rev. Lett. **96**, 226402 (2006).
[45]A. K. McMahan, K. Held, and R. T. Scalettar, Phys. Rev. B **67**, 075108 (2003).
[46]M. M. Rieger, L. Steinbeck, I. White, H. Rojas, and R. Godby, Comp. Phys. Commun. **117**, 211 (1999).
[47]L. Klasinc, A. Sabljic, G. Kluge, J. Rieger, and M. Scholz, J. Chem. Soc. Perkin Trans. **2**, 539 (1982).
[48]T. Pasinszki, M. Krebsz, and G. Vass, J. Mol. Struct. **966**, 85 (2010).
[49]P. Rademacher, K. Kowski, A. Mueller, and G. Bohlmann, J. Mol. Struct. **296**, 115 (1993).
[50]P. M. Mayer, V. Blanchet, and C. Joblin, J. Chem. Phys. **134**, 244312 (2011).
[51]T. Kobayashi, Z. ichi Yoshida, H. Awaji, T. Kawase, and S. Yoneda, Bull. Chem. Soc. Jpn. **57**, 2591 (1984).
[52]M. S. Deleuze, L. Claes, E. S. Kryachko, and J.-P. Francois, J. Chem. Phys. **119**, 3106 (2003).
[53]P.-K. Lo and K.-C. Lau, J. Phys. Chem. A **115**, 932 (2011).
[54]F. Bruneval, F. Sottile, V. Olevano, R. Del Sole, and L. Reining, Phys. Rev. Lett. **94**, 186402 (2005).
[55]M. Shishkin, M. Marsman, and G. Kresse, Phys. Rev. Lett. **99**, 246403 (2007).
[56]M. L. Tiago, S. Ismail-Beigi, and S. G. Louie, Phys. Rev. B **69**, 125212 (2004).
[57]K. Delaney, P. García-González, A. Rubio, P. Rinke, and R. W. Godby, Phys. Rev. Lett. **93**, 249701 (2004).
[58]M. Jurvansuu, A. Kivimäki, and S. Aksela, Phys. Rev. A **64**, 012502 (2001).
[59]M. Drescher, M. Hentschel, R. Kienberger, M. Uiberacker, V. Yakovlev, A. Scrinzi, T. Westerwalbesloh, U. Kleineberg, U. Heinzmann, and F. Krausz, Nature (London) **419**, 803 (2002).
[60]P. Liao and E. A. Carter, Phys. Chem. Chem. Phys. **13**, 15189 (2011).
[61]J. M. Luttinger and J. C. Ward, Phys. Rev. **118**, 1417 (1960).
[62]A. Klein, Phys. Rev. **121**, 950 (1961).
[63]C.-O. Almbladh, U. V. Barth, and R. V. Leeuwen, Int. J. Mod. Phys. B **13**, 535 (1999).
[64]V. M. Galitskii and A. B. Migdal, Sov. Phys. JETP **7**, 96 (1958).
[65]K. Delaney, Ph.D. thesis, University of York, 2003.
[66]F. Caruso, D. R. Rohr, M. Hellgren, X. Ren, P. Rinke, A. Rubio, and M. Scheffler, Phys. Rev. Lett. **110**, 146403 (2013).
[67]X. Ren, P. Rinke, C. Joas, and M. Scheffler, J. Mater. Sci. **47**, 7447 (2012).
[68]X. Ren, P. Rinke, G. E. Scuseria, and M. Scheffler, Phys. Rev. B **88**, 035120 (2013).
[69]D. Feller and K. A. Peterson, J. Chem. Phys. **110**, 8384 (1999).
[70]http://cccbdb.nist.gov/.
[71]M. Shishkin and G. Kresse, Phys. Rev. B **75**, 235102 (2007).
[72]G. Strinati, Riv. Nuovo Cimento **11**, 1 (1988).
[73]P. García-González and R. W. Godby, Phys. Rev. B **63**, 075112 (2001).
[74]B. Liu and A. D. McLean, J. Chem. Phys. **59**, 4557 (1973).